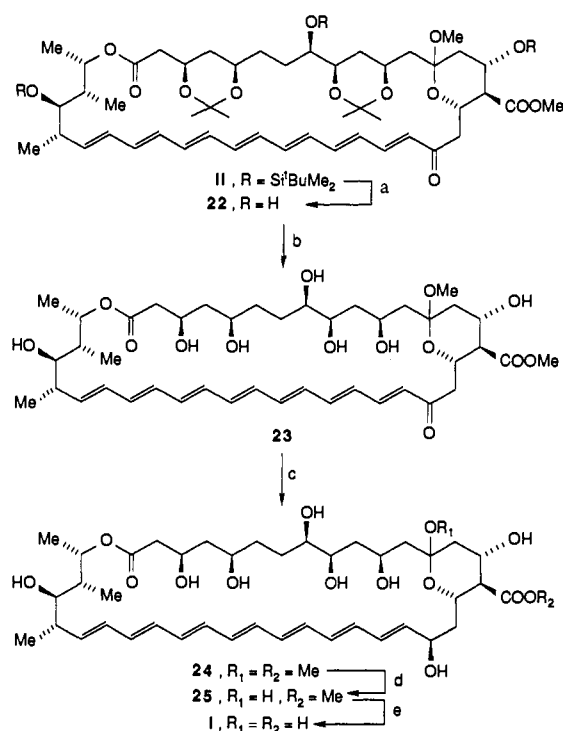


Scheme III<sup>a</sup>

<sup>a</sup> Reagents and conditions. (a) excess HF-pyr, MeOH, 45 °C, 48 h, 55%. (b) 0.1 equiv of CSA, MeOH, 0–25 °C, 1 h, 50% based on recovered starting material (10%) and a monoacetonide (25%, as yet unidentified isomeric structure). (c) 10 equiv of NaBH<sub>4</sub>, MeOH, 0 °C, 98%. (d) 0.1 equiv of CSA, MeOH–H<sub>2</sub>O (9:1), 0–25 °C, 97%. (e) 10.0 equiv of 1 N LiOH, H<sub>2</sub>O, 0–25 °C, 1 h, 80% (75% conversion).

and the resulting hydroxy acid was converted to the dimethyl ester **20** by sequential methylation (CH<sub>2</sub>N<sub>2</sub>), PDC oxidation, and a second methylation (CH<sub>2</sub>N<sub>2</sub>) (76% overall yield). The acetate was then removed from **20** (95%) and the carboxylic acid **21** was obtained by PDC oxidation of the resulting primary alcohol (79%). Finally, differentiation among the three carboxyl groups in **21** (anion formation at C-1, steric congestion at C-16) was observed in the one-step, chemoselective conversion of this intermediate to the requisite keto phosphonate acid III by attack of dimethyl (lithiomethyl)phosphonate at C-19 (62%). The second requisite key intermediate, hydroxy aldehyde IV, was constructed from synthetic VIII<sup>3</sup> and two units of phosphonate IX (Scheme I) as recently described.<sup>8</sup> Finally, coupling of III and IV (esterification, 70%) followed by macrocyclization (intramolecular keto phosphonate-aldehyde condensation, 70%) according to the procedures recently reported from these laboratories<sup>8</sup> led to heptaenone II.<sup>9</sup> Heptaenone II was then converted to I as outlined in Scheme III. Thus, desilylation of II (HF-pyr–MeOH) afforded triol **22** (55%), which was then subjected to deacetonization (CSA–MeOH) leading to heptahydroxy heptaenone **23** (50% yield based on ca. 50% conversion). Sodium borohydride reduction of **23** led, stereospecifically,<sup>1</sup> to the amphoteronolide derivative **24** (98%). The 19*R* configuration of the reduction product was confirmed by CD studies<sup>1</sup> and by comparisons of materials derived from **24** and amphotericin B.<sup>10</sup> Finally, sequential demethylation of **24** (CSA–MeOH, 97% followed by LiOH hydrolysis, 80% yield based on ca. 75% conversion) led to amphoteronolide B (**1**)<sup>11</sup> via its

(8) Nicolaou, K. C.; Chakraborty, T. K.; Daines, R. A.; Simpkins, N. S. *J. Chem. Soc., Chem. Commun.* 1986, 413.

(9) Both synthetic II and degradatively derived<sup>8</sup> II (two methoxy anomers, chromatographically separated) were found to be spectroscopically and chromatographically identical. Compounds **11–21** and III were carried through the sequence as mixtures of methoxy anomers.

(10) Nicolaou, K. C.; Daines, R. A.; Chakraborty, T. K.; Ogawa, Y. *J. Am. Chem. Soc.*, in press.

methyl ester **25**. Thus, the total synthesis of amphoteronolide B (**1**) was accomplished.<sup>12</sup>

**Acknowledgment.** We express our many thanks to Dr. C. Cimarusti, The Squibb Institute for Medical Research, for generous samples of amphotericin B, and to Drs. George Furst, Patrick Carroll, and John Dykins for their superb NMR, X-ray crystallographic, and mass spectroscopic assistance. This work was financially supported by the National Institutes of Health, Merck Sharp and Dohme, and Hoffmann-La Roche.

**Supplementary Material Available:** Listing of  $R_f$ ,  $[\alpha]_D$ , IR, UV, and <sup>1</sup>H NMR data for compounds **4**, **8**, **9**, **14**, **17**, **19**, **21**, II, III, IV, and **25** and a <sup>13</sup>C NMR spectrum of **25** (7 pages). Ordering information is given on any current masthead page.

(11) After chromatographic purification (silica, 25–75% MeOH in CH<sub>2</sub>Cl<sub>2</sub>) and spectroscopic characterization, the aglycon I was methylated (CH<sub>2</sub>N<sub>2</sub>, Et<sub>2</sub>O–Me<sub>2</sub>SO, 25 °C) back to amphoteronolide B methyl ester, identical with an authentic sample, thus further confirming its structure.

(12) All new compounds exhibited satisfactory spectral and analytical/exact mass spectral data. Yields refer to spectroscopically and chromatographically homogeneous materials.

### Preparation and Structure of (NEt<sub>4</sub>)<sub>2</sub>[V<sub>4</sub>S<sub>2</sub>(SCH<sub>2</sub>CH<sub>2</sub>S)<sub>6</sub>] and Its Structural and Electronic Relationship to the Li<sub>x</sub>VS<sub>2</sub> Phases

Joanna K. Money, John C. Huffman, and George Christou\*

Department of Chemistry and the  
Molecular Structure Center, Indiana University  
Bloomington, Indiana 47405

Received October 15, 1986

The polymeric sulfides of the early transition metals often display interesting magnetic and electrical properties<sup>1,2</sup> and have proven to be of considerable importance to many areas, not least of which are heterogeneous catalysis<sup>3</sup> and employment as battery electrodes.<sup>4</sup> A current and important challenge to the synthetic inorganic chemist is the preparation of soluble, discrete structural counterparts of the polymeric metal–sulfide phases to allow parallel characterization of both the reactivity characteristics in homogeneous solution and the intrinsic properties of the basic building block of the extended lattice. Such efforts have resulted in considerable progress, particularly in the chemistry of soluble molybdenum sulfides.<sup>5</sup> We herein report the preparation and properties of the first tetranuclear vanadium–sulfur–thiolate species. We believe this complex presages a rich new area of high nuclearity V/S/SR chemistry. In addition, we describe its structural and electronic correspondence to the Li<sub>x</sub>VS<sub>2</sub> polymeric phases (0 ≤ x ≤ 1).<sup>6</sup>

Reaction of VCl<sub>3</sub>, Li<sub>2</sub>S, Na<sub>2</sub>edt (edt is ethane-1,2–dithiolate), and NEt<sub>4</sub>Br in a 3:4:3:6 ratio in MeCN yields an intensely brown solution that, after filtration and addition of diethyl ether, deposits large black prismatic crystals of (NEt<sub>4</sub>)<sub>2</sub>[V<sub>4</sub>S<sub>2</sub>(edt)<sub>6</sub>]·2MeCN in analytical purity.<sup>7</sup> A single-crystal structure determination<sup>7</sup> shows the anion (Figure 1) to possess a V<sub>4</sub>S<sub>2</sub> central core with two

(1) Hullinger, F. *Struct. Bonding (Berlin)* 1968, 4, 83.

(2) Whittingham, M. S. *J. Electrochem. Soc.* 1976, 123, 315.

(3) Weisser, O.; Landa, S. *Sulfide Catalysts: Their Properties and Applications*; Pergamon: New York, 1973.

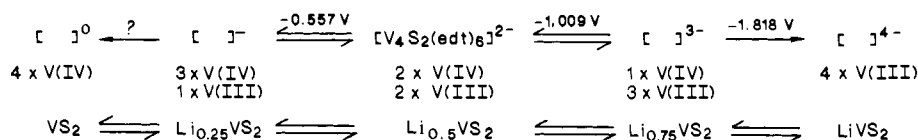
(4) Rouxel, J.; Brec, R. *Annu. Rev. Mater. Sci.* 1986, 16, 137–162.

(5) Muller, A. *Polyhedron* 1986, 5, 323.

(6) Murphy, D. W.; Cros, C.; DiSalvo, F. J.; Waszczak, J. V. *Inorg. Chem.* 1977, 16, 3027.

(7) Crystallographic data at –155 °C: triclinic; space group  $P\bar{1}$ ;  $a = 11.130$  (3),  $b = 11.424$  (3),  $c = 10.748$  (3) Å;  $\alpha = 112.04$  (1),  $\beta = 94.82$  (1),  $\gamma = 93.44$  (1)°;  $Z = 1$ ;  $R = 0.0459$ ,  $R_w = 0.0467$ , using 3290 unique intensities with  $F > 3\sigma(F)$ . All non-hydrogen atoms were refined anisotropically; hydrogen atoms were located in a difference Fourier and refined isotropically. Anal. Calcd for C<sub>32</sub>H<sub>70</sub>N<sub>4</sub>S<sub>14</sub>V<sub>4</sub>: C, 33.03; H, 6.06; N, 4.82. Found: C, 32.77; H, 6.01; N, 4.60.

## Scheme I



$\mu_3$ -sulfur atoms S(3) and S(3'), one above and one below an exactly planar  $V_4$  parallelogram; the anion possesses an imposed inversion center. Peripheral ligation is accomplished by six  $edt^{2-}$  groups that separate into three types defined by their sulfur binding modes: (i) with both sulfur atoms terminal, S(12) and S(15), (ii) with both sulfur atoms bridging, S(4) and S(7), and (iii) with one sulfur bridging, S(8), and one sulfur terminal, S(11). Each type occurs in symmetry-related pairs. The vanadium atoms possess distorted octahedral geometry, and consideration of overall anion charge necessitates the mixed-valence description V(III,III,IV,IV). Based on inspection of structural parameters, however, there is no justification for a trapped-valence description, and the anion is best described as electronically delocalized with an average formal metal oxidation state of +3.5.<sup>8</sup>

The  $[V_4S_{14}]$  core of the  $[V_4S_2(edt)_6]^{2-}$  anion is very close to representing a discrete portion of the  $Li_xVS_2$  phases recently characterized<sup>6</sup> as possessing the layer structure of  $CdI_2$ . In  $Li_xVS_2$ , infinite sheets of octahedrally coordinated vanadium atoms are bridged by  $\mu_3$ - $S^{2-}$  atoms, alternatingly above and below the  $V_{\infty}$  plane, with  $Li^+$  ions in interlayer spaces. In  $[V_4S_2(edt)_6]^{2-}$ , ef-

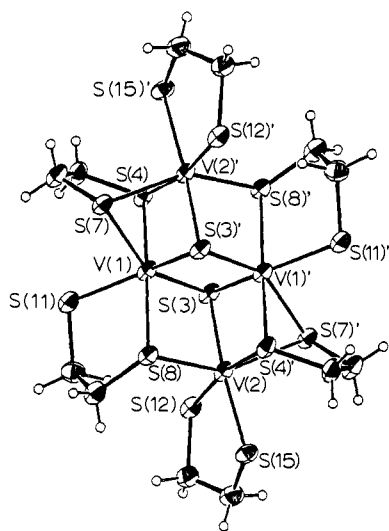


**Figure 1.** ORTEP projection of  $[V_4S_2(edt)_6]^{2-}$  showing the atom-labeling scheme. Selected bond lengths (Å) and angles (deg): V(1)–V(1'), 3.039 (1); V(1)–V(2), 3.300 (1); V(1)–V(2'), 2.771 (1); V(1)–S(3), 2.315 (2); V(1)–S(3'), 2.387 (2); S(3)–V(1)–S(3'), 99.49 (6); V(1)–S(3)–V(1'), 80.51 (6); V(1)–S(3)–V(2), 70.98 (6); V(1)–S(3)–V(2'), 69.20 (5).

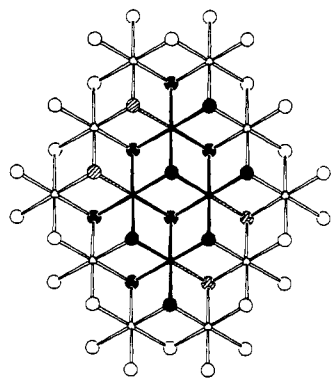


**Figure 2.** Portion of the two-dimensional extended lattice of the  $Li_xVS_2$  phases. Vanadium (●) and sulfur (○) atoms corresponding to those in  $[V_4S_2(edt)_6]^{2-}$  are indicated. The shaded (◐) sulfur atoms are those replaced by sulfurs S(7) and S(7') of the model complex.

fective replacement of peripheral sulfide atoms by thiolate sulfurs keeps the unit discrete and soluble (Figure 2). Thus, with the exception of S(7) and S(7'), all thiolate sulfur atoms are in positions<sup>9</sup> occupied by  $S^{2-}$  atoms in  $VS_2$ , which bridge to other metal atoms yielding an infinite lattice. The exception mentioned, S(7), replaces two  $S^{2-}$  atoms of the  $Li_xVS_2$  phases that bridge to additional metal centers.

$[V_4S_2(edt)_6]^{2-}$  also shows strong similarities to the  $Li_xVS_2$  phases by virtue of its variable electron content. The dianion, with its +3.5 average oxidation level, corresponds to  $Li_{0.5}VS_2$ ; in the cyclic voltammogram, a reversible one-electron oxidation at  $-0.557$  V and two one-electron reductions at  $-1.009$  and  $-1.816$  V (the first reversible) are observed.<sup>10</sup> These correspond to other oxidation levels of the  $Li_xVS_2$  phases, which have been prepared by varying the Li content (Scheme I; corresponding oxidation levels are presented in the same column).

The accessibility of  $[V_4S_2(edt)_6]^{0}$  cannot be confirmed because the region of the CV at  $> \sim 0$  V is masked by a multielectron oxidation wave probably due to ligand oxidation; nevertheless, the overall relationship is clear.

Several examples are known in inorganic chemistry of molecular species that can be considered discrete, soluble fragments of solid-state materials and that display similar variable electron content, but this has not hitherto been the case in metal–sulfide chemistry. The known examples<sup>11</sup> of discrete metal–sulfur aggregates that bear structural relation to polymeric materials either show no reversible redox behavior or, in cases where they do, have no counterpart to such behavior in the solid-state material. The anion  $[V_4S_2(edt)_6]^{2-}$  thus represents the first time that such a high degree of correspondence has been established between both the structure and the variable electron content of a solid-state metal–sulfide and its discrete fragment.

The  $Li_xVS_2$  phases have been shown to display unusual temperature-dependent magnetic properties and structural distortions as the Li content is varied.<sup>6</sup> Given the potential importance as battery electrodes of this and similar materials such as  $Li_xTiS_2$ ,<sup>4</sup> there is a resulting desire to obtain a deeper understanding of their magnetic, structural, and electronic properties. Availability of discrete structural forms should prove beneficial in allowing the corresponding magnetic, structural, and redox properties of the basic "repeating unit" to be assessed with ease. Such knowledge might be valuable in the future development of these conducting materials. With this in mind, we are currently attempting to isolate the mono- and trianionic forms of  $[V_4S_2(edt)_6]^{2-}$  to allow a parallel study of such properties for three oxidation levels.

**Acknowledgment.** This work was supported by NSF Grant CHE 8507748.

**Supplementary Material Available:** Tables of atomic coordinates and isotropic and anisotropic thermal parameters (3 pages). Ordering information is given on any current masthead page.

(8) The solid-state magnetic moment at 303 K was found to be  $2.43 \mu_B/V_4$  unit ( $1.21 \mu_B/V$ ), indicating magnetic interactions between the metal centers.

(9) We do not mean to imply by this wording that the sulfur atoms are in exactly the same positions. Note that the coordination geometries of the metal atoms in  $[V_4S_2(edt)_6]^{2-}$  are severely distorted octahedral, a situation not found in the much higher symmetry of the hexagonal lattice of a  $CdI_2$ -type structure.

(10) Measurements were performed in MeCN solution containing 0.1 M  $N(n-Bu)_4ClO_4$  as supporting electrolyte. Potentials are quoted vs. the normal hydrogen electrode using ferrocene (+0.400 V vs. NHE) as external standard.

(11) Christou, G.; Hagen, K. S.; Bashkin, J. K.; Holm, R. H. *J. Am. Chem. Soc.* **1985**, *24*, 1010. Choy, A.; Craig, D.; Dance, I.; Scudder, M. *J. Chem. Soc., Chem. Commun.* **1982**, 1246. Bogdanovich, B.; Goddard, R.; Gottsch, P.; Kruger, C.; Schlichte, K.; Tsay, Y.-H. *Z. Naturforsch., B.* **1979**, *34B*, 609.